European Journal of Pharmaceutics and Biopharmaceutics 206 (2025) 114582

Contents lists available at ScienceDirect

European Journal of Pharmaceutics and Biopharmaceutics

journal homepage: www.elsevier.com/locate/ejpb

Research paper

A multifaceted approach to understanding protein-buffer interactions in biopharmaceuticals

Blaž Lebar [a,b], Maria Orehova [d], Boštjan Japelj [b], Ernest Šprager [b], Rok Podlipec [c], Tilen Knaflič [c], Iztok Urbančič [c], Benjamin Knez [b], Mitja Zidar [b], Jure Cerar [b], Janez Mravljak [a], Aleš Žula [b], Denis Arčon [c], Janez Plavec [d], Stane Pajk [a,*]

[a] University of Ljubljana, Faculty of Pharmacy, Department of Pharmaceutical Chemistry, Aškerčeva 7, SI-1000 Ljubljana, Slovenia
[b] Novartis Pharmaceutical Manufacturing LLC, Kolodvorska 27, SI-1234 Menges, Slovenia
[c] Jožef Stefan Institute, Laboratory of Biophysics & Quantum Materials Group, Jamova cesta 39, SI-1000 Ljubljana, Slovenia
[d] National Institute of Chemistry, Slovenian NMR Centre, Hajdrihova ulica 19, SI-1000 Ljubljana, Slovenia

ARTICLE INFO

Keywords:
Monoclonal antibody
Interaction
Buffer
Nuclear magnetic resonance
Methyl fingerprinting
Molecular dynamics

ABSTRACT

The excipient selection process plays a crucial role in biopharmaceutical formulation development to ensure the long-term stability of the drug product. Though there are numerous options approved by regulatory authorities, only a subset is commonly utilized. Previous research has proposed various stabilization mechanisms, including protein-excipient interactions. However, identifying these interactions remains challenging due to their weak and transient nature. In this study, we present a comprehensive approach to identify such interactions. Using the ^{1}H T_2 CPMG (Carr-Purcel-Meiboom-Gill) filter experiment we identified interactions of rituximab with certain buffers and amino acids, shedding light on its Fc fragment instability that manifested during the enzymatic cleavage of the antibody. Moreover, chemometric analyses of 2D NMR fingerprints revealed interactions of selected excipients with antibody fragments. Furthermore, molecular dynamics simulations revealed potential interacting hotspots without NMR spectra assignment. Our results highlight the importance of an orthogonal methods approach to uncovering these critical interactions, advancing our understanding of excipient stabilization mechanisms and rational formulation design in biopharmaceutics.

1. Introduction

Monoclonal antibodies (mAbs) have revolutionized the treatment of various diseases, offering promising new therapies for conditions like autoimmune diseases and cancer [1]. However, developing stable liquid biopharmaceutical formulations, which are the most common form of biopharmaceuticals [2], particularly in the form of liquid injectable antibodies, demands careful selection of excipients that ensure the protein's chemical and physical stability.

Physical stability includes conformational stability, resistance of a protein to unfolding, and colloidal stability, the ability of a protein to remain in monomeric native form. Colloidal stability is affected by the formation of misfolded species, aggregation, and precipitation of proteins [3–5]. Understanding these instabilities and how excipients influence them is crucial for developing optimal mAb formulations.

Instabilities in biopharmaceutical formulations are mitigated through formulation development, where specific excipient combinations are carefully selected to mitigate risks, such as protein stability and solubility, immunogenicity, efficacy and potency, etc. Commonly used excipients include histidine as a buffering agent, sucrose for tonicity and stabilization, polysorbate 80 as a surfactant, arginine to reduce viscosity, and EDTA as a chelating agent. While a range of other excipients is also employed, either individually or in combination, the overall number remains relatively limited compared to the full spectrum of FDA-approved excipients. A buffering excipient is not used for some high-concentration antibody formulations due to the intrinsic buffering capacity of the antibody [6].

Various mechanisms underlie the stabilization of proteins in biopharmaceuticals formulations. Buffers primarily control pH to prevent unwanted deamidations and oxidations of the amino acids and also provide physical stability by influencing charge repulsion [7,8]. However, specific buffer species exert distinct effects, either stabilizing or

* Corresponding author.
E-mail address: stane.pajk@ffa.uni-lj.si (S. Pajk).

https://doi.org/10.1016/j.ejpb.2024.114582
Received 23 May 2024; Received in revised form 15 November 2024; Accepted 18 November 2024
Available online 19 November 2024

destabilizing on the protein [9], inducing gelation [10], or interacting with antibodies [11].

Understanding these interactions is crucial, as various excipients interact with proteins in numerous ways: electrostatic interactions (e.g., with polyanions – heparin and positively charged patches on the protein), cation–π (e.g., arginine-aromatic residues) and hydrophobic interactions (e.g., polysorbate with exposed hydrophobic regions on the protein surface). Additional interactions include hydrogen bonding, van der Waals interactions and CH– π, among others [11,12].

A plethora of studies in the literature delve into interactions between therapeutic proteins and excipients. Arginine, widely recognized as the viscosity reducing agent and occasionally as a protein aggregation suppressor [13–15], has been shown to interact with proteins in multiple studies [16–20]. Citrate has been demonstrated to interact with the Fab domain of the antibody [21], while phosphate has been associated with increased thermostability and melting temperature (T_M) of various proteins [22,23], though this effect is not universal. Surfactant interactions, namely polysorbate 20 and 80, have also been extensively explored. Polysorbate's interaction with darbepoetin alfa and recombinant human growth hormone has been confirmed [24,25]. Histidine has been identified to provide non-covalent stabilizing interactions with antibodies in the solid state [26] and hypothesized that the stabilizing effect of proline in the formulation of human normal immunoglobulin (SCIg) might arise from proline's binding to exposed hydrophobic protein domains, preventing harmful aggregation [27].

Protein-excipient interactions are often weak and transient with dissociation constants K_d in the *mM* range [28], rendering standard methods like isothermal titration calorimetry (ITC) and surface plasmon resonance (SPR) insufficiently sensitive [29,30]. Nuclear magnetic resonance (NMR), due to its high sensitivity, has emerged as a powerful tool for probing these interactions.

Previous studies have successfully employed various 1D NMR techniques like saturation transfer difference (STD), Carr-Purcel-Meiboom-Gill (CPMG) and WaterLOGSY to identify excipient interactions with model proteins [31]. This study utilizes the $^1H\ T_2$ CPMG filter experiment, which leverages the increased relaxation rate of excipients upon binding to larger proteins [48]. This approach allows us to directly observe differences in transverse relaxation of excipient protons in the presence and absence of the protein, offering a sensitive probe for analyzing protein-excipient interactions.

While studying the interactions described above with 2D NMR holds immense potential, the inherent size and complexity of these molecules historically posed significant challenges due to faster magnetization relaxation. Recent advancements in NMR technology, including more powerful equipment, modern pulse sequences, and improved methods have paved the way for exploring of these interactions in larger molecules.

Pioneering work by Arbogast et al. ($^1H{-}^{13}C$) and Brinson et al. ($^1H{-}^{15}N$) established the use of 2D NMR fingerprinting, offering valuable insights into protein structure and stability [32,33]. Originally, it was developed as a tool for biopharmaceutical development, where higher order structure (HOS) of unlabeled antibodies can be determined and used as drug quality criteria. Further studies demonstrated the potential of this technique in identifying binding sites for excipients like polysorbates in mAb fragments, utilizing cross-peak volume loss and chemical shift perturbations, respectively [34,35]. However, another study using 2D NMR fingerprint highlights the nuance of these interactions, suggesting that not all excipients exhibit site-specific binding with all proteins [36].

Recent advancements in the described field utilize *in silico* approach, offering valuable tools for exploring the interactions at an atomic level. Shukla et al. pioneered the use of preferential interaction coefficient Γ_{23}, derived from molecular dynamics simulations [37]. This approach was later employed by Cloutier et al. to evaluate interactions between three monoclonal antibodies and various excipients [38,39], connecting the simulations to experimental observation on aggregation and viscosity. Their work included spatial aggregation propensity (SAP) [40] and spatial charge map (SCM) [41] for comprehensive analysis. Another study utilized molecular dynamics (MD) simulations to evaluate the stabilizing effects of histidine on full mAbs and their fragments [42].

This study elucidates protein-buffer interactions, crucial for the stability of biopharmaceutical formulations yet challenging to characterize due to their weak and transient nature. Rituximab, as the model mAb, was cleaved and purified to obtain Fab and Fc fragments, allowing for a more detailed characterization of interactions later in the study. A comprehensive suite of complementary analytical methods was employed. We demonstrated the effectiveness of $^1H\ T_2$ CPMG filter experiments in detecting interactions that correlate with observations of Fc region instability and stabilizer efficiency. Additionally, the application of methyl and amide fingerprint, leveraging the natural abundance of ^{13}C and ^{15}N isotopes, has proven particularly effective in revealing these subtle interactions. The use of chemometric techniques, specifically principal component analysis (PCA) and combined chemical shift deviation (CCSD), has proven effective in discerning spectral variations. *In silico* methods were also implemented to further support the interactions observed with previous techniques. This study advances the understanding of protein-buffer interactions by evaluating a multifaceted methodological approach, offering new approach for analyzing these critical interactions in biopharmaceutical development.

2. Materials and methods

2.1. Chemicals and materials

The following chemicals were obtained from Sigma-Aldrich, Merck KgA (Darmstadt, Germany): Acetic acid (glacial), Citric acid, Deuterium oxide D_2O (99.9 % D), Hydrochloric acid 25 %, L-Arginine, L-Histidine, L-Lysine Monohydrochloride, Sodium hydroxide pellets, Succinic acid and Sucrose. Ultrapurified water (UPW) was used for sample preparation.

Following materials were used: FabALACTICA (cysteine protease IgdE) Immobilized Microspin Kit was obtained from Genovis (Lund, Sweden), Slide-A-Lyzer™ Dialysis Cassettes, 10 K MWCO from Thermo Fisher Scientific Inc. (Waltham, MA, USA) and Amicon® Ultra Centrifugal Filter, 10 kDa MWCO from Sigma-Aldrich, Merck KgA (Darmstadt, Germany).

Rituximab (called mAb in paper) was used as a model monoclonal antibody, and was supplied by Novartis (Mengeš, Slovenia).

2.2. Analytical size exclusion chromatograpy (SEC)

Samples were analyzed using a Waters ACQUITY UPLC system at 40 °C, employing a SEC column with dimensions of 4.6 mm × 150 mm and a pore size of 200 Å, containing 1.7 µm beads. A sample volume of 0.75 µL was injected. The mobile phase, comprising 50 mM sodium dihydrogen phosphate and 400 mM sodium perchlorate at pH 6.0, was delivered at a flow rate of 0.4 mL/min, with a total run time of 5 min. Prior to injection, samples were diluted to 1 mg/mL in 150 mM sodium phosphate buffer at pH 7 and stored at 2–8 °C in the autosampler. Data analysis was performed using Empower 3 software. The variability of the relative aggregate content measurement (aggregates/monomer) at the specified column loading was estimated to be 0.05 %. Samples were measured within the linear range of detection, following the standard established analytical method at Novartis. Integration of peaks was limited to those above the quantification threshold. The upper limit was not reached using the same procedure.

2.3. mAb cleavage and purification

mAb was cleaved by cysteine protease IgdE immobilized on a column

following the manufacturers manual. Site of cleavage was above the hinge region producing one Fc fragment and two Fab fragments from one full mAb. Efficiency of cleavage was monitored by sampling the mAb before and after the cleavage with analytical SEC. To separate cleaved fragments, two-step purification was performed on final solution from IgdE cleavage.

The protein purification experiments were performed on an ÄKTA Avant 25 (Cytiva, Massachusetts) consisting of two system pumps, a sample pump, a UV detector with a 0.2-cm flow cell, a pH monitor, and a conductivity detector. Fractions were collected with an integrated and cooled fraction collector into 15–mL falcon tubes. The system was controlled with Unicorn 7.2 software (Cytiva, Massachusetts, USA). Protein A affinity chromatography (ALC) column, packed with MabSelectSure (Cytiva, Massachusetts) resin at 20 cm bed height and 1.6 cm diameter, and size exclusion chromatography (SEC) column, packed with Superdex®200 Prep Grade (Cytiva, Massachusetts) resin at 60 cm bed height and 1.6 cm diameter and were used for protein separation. Final solution from IgdE cleavage was loaded onto a Protein A affinity column at 300 cm/h flow rate and at a column load of 18 $mg_{protein}/mL_{resin}$. Column was washed with 3 column volumes of wash buffer (50 mM sodium phosphate, pH 7) and unbound Fab fragments (unbound fraction) were collected during load and wash step. Bound uncleaved mAb and Fc fragments (bound fraction) were eluted with 5 column volumes of elution buffer (50 mM sodium acetate, pH 3.6). Eluted fraction was then applied onto SEC column operated at 120 cm/h flow rate in 20 mM sodium-phosphate, pH 6.2. Injection volume was 2 ml with column load of 0.7 $mg_{protein}/mL_{resin}$. Whole elution peak was fractionated, and purity of fractions was checked with SEC–UPLC. Only fractions with sufficent Fc purity were pooled. Multiple runs of cleavage and purification were performed to ensure sufficient quantities of fragments.

Fab and Fc fragments were separately dialysed into UPW using Slide-A-Lyzer™ Dialysis Cassettes, 10 K MWCO and subsequently concentrated to desired concentration using Amicon® Ultra Centrifugal Filter, 10 kDa MWCO. Integrity of both proteins was monitored using analytical SEC, to ensure that no fragmentation or aggregation occurred during the process.

2.4. NMR measurements

NMR experiments were performed on Bruker AVANCE NEO 600 MHz (1D experiments) and 800 MHz (1D and 2D experiments) NMR spectrometers equipped with triple-resonance cryogenic probe heads. All samples contained 10 % of D_2O. The detected frequencies for ^1H nuclei were referenced against the external DSS standard. The detected frequencies for ^{13}C and ^{15}N nuclei were indirectly referenced using gyromagnetic ratios and directly referenced ^1H nuclei frequencies. Obtained NMR spectra were processed with Topspin 4.1.3 or NMRPipe and visualized with Sparky software.

Differences in transverse relaxation rates of protons excipients were measured at 25 °C using ^1H T_2 CPMG filter experiments. Spectra were recorded for proteins, each of excipients and for mixtures excipient-protein with molar ratio 10:1 and 100:1. An inter-scan delay was set to 3.0 s, 32 transitions were used for each spectrum, number of CPMG loops was set to $L = 1$ and $L = 128$. Water suppression was achieved using excitation sculpting method. Heights of selected resonances of excipients were compared between spectra with $L = 1$ and $L = 128$. Prior to comparison, from the spectra with L = 1 at excipient-protein molar ratio 10:1 corresponding spectrum of protein alone was subtracted in order to avoid influence on the results from the overlap with protein resonances.

^1H–^{13}C heteronuclear single quantum coherence (HSQC) 2D spectra for methyl protons were recorded at 50 °C, with 2048 × 560 data points in the direct and indirect dimensions, respectively. 96 transitions were used for each spectrum. Spectral width was 11.37 ppm in direct dimension and 80 ppm in indirect dimension. The ^{1}H carrier was set to 4.7 ppm and ^{13}C carrier was set to 40 ppm. An inter-scan delay was 1.5 s, non-uniform sampling was applied for data acquisition. NUS data reconstruction was performed using standard Topspin algorithms (or NMRPipe).

^1H–^{15}N saturation optimized and fast acquisition heteronuclear multiple quantum coherence (SOFAST HMQC)spectra were acquired at 50 °C with 2048 × 256 data points in the direct and indirect dimensions, respectively. 1472 transitions were used for each spectrum. Spectral width was 15.6 ppm in direct dimension and 35 ppm in indirect dimension. The ^1H carrier was set to 4.7 ppm and ^{15}N carrier was set to 117 ppm. An inter-scan delay was 0.1 s. Selective ^1H excitation pulse with the offset of 9 ppm and bandwidth of 5.2 ppm was applied.

2.5. In silico

2.5.1. Computational modelling and molecular dynamics simulations

The mAb structure was constructed via homology modeling utilizing IgG1 template (PDB: 1HZH [43]) with the Schrodringer BioLuminate suite [44]. Full mAb structure was split into Fc and Fab parts by saving them as separate pdb files in Chimera 1.16.MD simulations (MD) were conducted using GROMACS 2022.2 software [45]. The system was parametrized with the OPLS all-atom force field model [46] with TIP3P [47] water model. One mAb molecule was positioned within a triclinic simulation box with periodic boundary conditions, ensuring a minimum distance of 2.0 nm from protein surface. Subsequently, the system was supplemented with water molecules and randomly placed appropriate number of excipients molecules in their correct protonation state, depending on the desired concentration and pH. Neutralization of the system's charge was achieved by adding Na^+ and/or Cl^- ions. The protonation states of titratable groups were adjusted to the target pH of using the PROPKA3.5 protocol [48]. Simulations were performed under the *NpT* ensemble conditions, with a constant pressure of 1 atm and a temperature of 300 K. Initial relaxation of the systems was carried out through approximately 1000 steps of steepest descent minimization algorithm, followed by production runs of 110 ns (or longer). The first 10 ns of each trajectory were discarded as equilibrium and configurations were saved approximately every 100 ps, yielding 1000 uncorrelated snapshots for subsequent calculations and analysis.

2.5.2. Protein-excipient interaction calculation

The mAb's (or fragment's) interaction with test compounds was assessed using the concept of the radial distribution function (RDF), $g(r)$, which depicts the spatial density distribution of a test particle around a reference particle. This function is normalized to 1 at infinite distances (representing bulk density), with deviations indicating changes in particle density at specific distance. To pinpoint regions on the mAb surface with potential interaction sites, RDF calculations were conducted for each amino acid in the mAb's sequence (serving as the reference particle) in relation to all tested excipients. The distance for the calculation from the amino acid (r) was segmented into 75 bins, with a cutoff at 15 Å. Quantifying the interaction level between an amino acid and excipient ($I_{AA,exc}$), involved computing the integral $I_{AA,exc} = \int_{r=0\,Å}^{r=15\,Å} g(r)dr$, which measures the excipients presence around the amino acid. Computational analyses employed custom Python scripts, leveraging PyMOL 2.5.2 (Schrödinger LCC 2020), and MDAnalysis 2.4.3 packages [49]. Visualizations were created using PyMOL.

2.6. Chemometric analysis

2.6.1. Principal component analysis (PCA)

Principal component analysis was performed using the input matrix consisting of ^1H and ^{13}C chemical shifts and peak intensities using prcomp function, which uses single value decomposition and factoextra package for visualization of scores in R programming language [50,51].

A custom function was written to reshape the data for each pH value and connect the edges of the triangles in the plot.

2.6.2. Sequential nearest neighbors graph invariants (SNN-GI)

SNN-GI algorithm was programmed in R programming language based on a paper [52]. The algorithm uses map invariants, i.e numerical descriptors that neither depend on assumed numbering of protein spots nor depend on the orientation of the map. The peaks are first ordered with respect to decreasing intensities. Then each cross peak is connected to the n-nearest neighbor(s) (for $NN = 1to6$) cross peak if the neighbor has lower order, i.e. higher intensity. This can be done by calculating distance-adjacency matrix for each cross peak, which is sparse. The further details of calculations are described in [52,53].

2.6.3. Combined chemical shift deviation (CCSD)

CCSD were computed using the equation: $CCSD = \sqrt{\frac{1}{2} \bullet \left(\left(\delta_H - \delta_{H,ref}\right)^2 + \alpha^2 \left(\delta_X - \delta_{X,ref}\right)^2 \right)}$, where δ_H and δ_X are ^1H and ^{13}C chemical shifts in ppm, respectively. $\delta_{H,ref}$ and $\delta_{X,ref}$ are the chemical shifts of the same cross peak in the reference spectra. α is scaling factor to normalize the ppm ranges of the ^1H and ^{13}C nuclei (0.251 for ^{13}C) [33,54,55].

3. Results and discussion

3.1. mAb cleavage and purification

Cysteine protease IgdE efficiently cleaved mAb above hinge region, yielding a Fc fragment and two Fab fragments. Due to incomplete cleavage, some intact mAb and semi-cleaved mAb remained (Fig. 1). However, following optimized incubation times, less than 10 % of full mAb and less than 20 % of semi-cleaved mAb were still present after cleavage. Subsequent purification steps using sequential preparative protein A affinity chromatography (ALC) and SEC successfully isolated pure Fab and Fc fragments (Fig. S1 and S2). Importantly, both the cleavage and purification processes maintained the stability of mAb fragments. The final purities of the Fab and Fc fragments were 99.2 % and 97.6 %, respectively.

The successful isolation of highly purified fragments, with their smaller sizes compared to the intact mAb, facilitated high-resolution NMR measurements. By overlaying these spectra and applying rigorous chemometric analysis (detailed later in the paper), we were able to precisely identify and characterize changes in the higher-order structure (HOS) of the individual fragments compared to the intact mAb.

3.2. Fc fragment instability at increased pH and stabilizers

Following IgdE cleavage, the isolated Fc fragment exhibited pH-dependent instability, reversibly precipitating above pH 6. To evaluate the effectiveness of various stabilizers, we monitored the protein solution for signs of precipitate formation. We tested excipients that are regularly used in formulation stabilization: lysine chloride (LysCl), arginine chloride (ArgCl), sodium citrate (NaCit), and sodium succinate (NaSucc). Initially, the pH was adjusted to 6, and each excipient was added to a final concentration of 10 mM. Observations were conducted 48 h post-addition; however, in cases where precipitation occurred, it was immediate and remained unchanged over the 48-h period. The excipient concentration was subsequently increased to 100 mM, and the solutions were re-examined (Table 1). The control sample consisted of the Fc fragment in ultrapure water (UPW) with a volume of UPW added to match the dilution in the excipient-treated samples. All tested excipients, with the exception of lysine chloride and arginine chloride (effective only at 100 mM), successfully stabilized the Fc fragment at a 10 mM concentration, suggesting potential stabilizing interactions between the Fc fragment and these compounds. This hypothesis is explored further in the article.

3.3. Buffers and Fc stabilizers

In this chapter our goal was to evaluate methods to detect interactions between mAb fragments and excipients. Beside stabilizers from section 3.2, histidine and acetate buffers were also tested due to their prevalence in biopharmaceutical formulation development.

3.3.1. CPMG

^{1}H T_2 CPMG filter experiments for protein formulations with set of charged excipients in presence of sodium acetate buffer (pH 6.0) were performed (Table S1). No differences in relaxation rate were observed for acetate at both excipient-protein molar ratios 10:1 or 100:1. On the contrary, significantly faster relaxation was observed for succinate and citrate protons at excipient-protein molar ratio 10:1. Prominent increase in relaxation rate was also observed for amino acid excipients histidine, lysine and arginine at excipient-protein molar ratio 10:1, of which the smallest effect was detected for arginine. The decrease in resonance intensity is more prominent in the presence of protein for citrate and histidine buffer (Fig. 2). The results suggest that tested di- and tricarboxylic acids anions, as well as all three amino acids interact with the protein surface. Interactions with mentioned excipients agree with Fc stabilisation results in previous paragraph.

3.3.2. Methyl fingerprinting

Methyl fingerprinting ($^1H{-}^{13}C$) detects methyl group from six amino acids' (Ala, Val, Leu, Ile, Met and Thr) side chains. Although limited in amino acid coverage, this method provides valuable information about excipient proximity and changes in protein HOS due to the

Table 1
Precipitation of the Fc fragment in various buffer solutions and ultrapure water (UPW) at two excipient concentrations (10 mM and 100 mM). Presence of precipitation is indicated by "+", and absence by "-".

	Fc precipitation	
Buffer	**10 mM**	**100 mM**
LysCl	+	−
ArgCl	+	−
NaCit	−	−
NaSucc	−	−
UPW	+	+

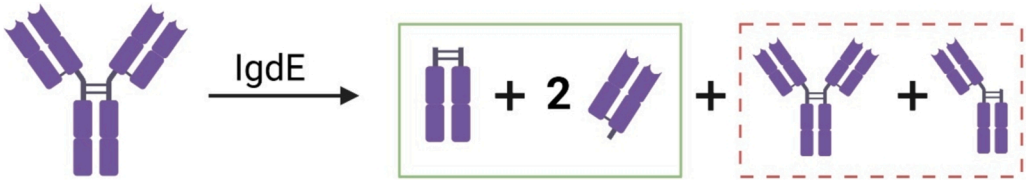

Fig. 1. IgdE cleavage scheme. Full cleavage produces one Fc and two Fab fragments, cleaving above hinge region (green box). Imperfect Incomplete reaction also yields uncleaved and semi-cleaved mAb (dashed red box) that needed to be removed during purification steps. (For interpretation of the references to color in this figure legend, the reader is referred to the web version of this article.)

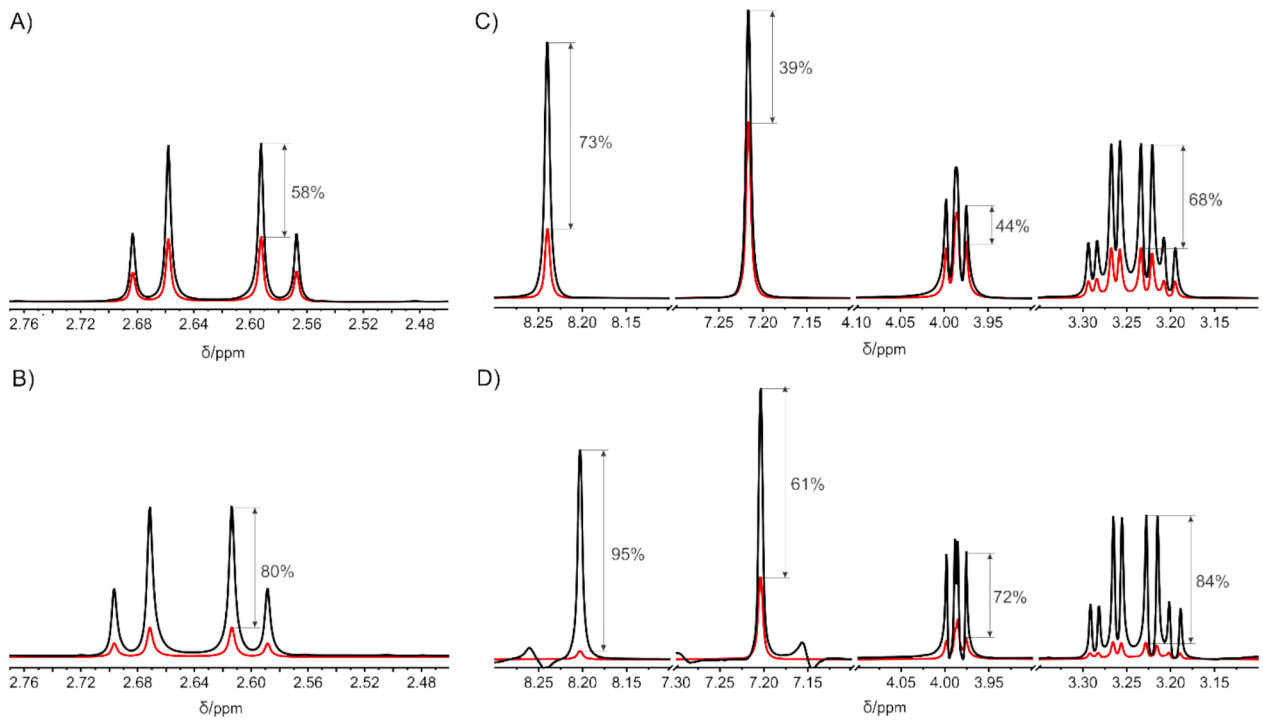

Fig. 2. Comparison of intensity decrease of excipient resonances in the absence and in the presence of protein (excipient:protein molar ratio 10:1) (A) citrate; (B) citrate + protein; (C) histidine; (D) histidine + protein. Spectra were recorded at 25 °C on 600 MHz NMR spectrometer.

unique chemical environment of each methyl group. Distinct spectral regions for ^{1}H and ^{13}C resonance and high natural abundance of ^{13}C enable good spectral resolution with reasonable acquisition times [32].

Methyl fingerprints of Fab fragment were recorded in histidine chloride buffer (His/HCl), sodium acetate buffer (Na/Ac) and without buffering excipients (WBE), all at pH 9, 7, 6 and 5 (producing total of 12 fingerprints). Fc fragment fingerprints employed same three buffers, but at pH 6, 5 and 4 (producing total of 9 fingerprints). Fc fragment was also recorded in formulation without buffering excipients at pH 5.5, but with arginine, lysine and succinate as stabilizers (3 fingerprints in total). Amide fingerprints of Fab were recorded only, with sodium acetate and formulation without buffering excipients at both pH 5 and 7 (total of 4 fingerprints).

Table 2 summarizes all recorded methyl and amide spectra recorded in this study. Full assignment of these spectra was not in scope of this study. Instead, we employed a technical assignation approach, which proved sufficient for evaluating the methods tested. Ideally, full assignment would identify the specific amino acids involved in interactions. Spectra were recorded at 0.6 mM protein concentration, ensuring sufficient buffering capacity for stable pH in formulations without buffering excipients.

Table 2
Summary of all 2D NMR spectra recording. WBE denotes formulation without buffering excipients. Included are amide fingerprint spectra addressed in section 3.3.4.

Fragment	Type and number of fingeprints recorded	Buffer (secondary excipient)	pH of measurement
Fab	Methyl (4)	His/HCl	5, 6, 7, 9
	Methyl (4)	Na/Ac	5, 6, 7, 9
	Methyl (4)	WBE	5, 6, 7, 9
Fc	Methyl (3)	His/HCl	4, 5, 6
	Methyl (3)	Na/Ac	4, 5, 6
	Methyl (3)	WBE	4, 5, 6
	Methyl (1)	WBE (arginine)	5.5
	Methyl (1)	WBE (lysine)	5.5
	Methyl (1)	WBE (succinate)	5.5
Fab	Amide (2)	Na/Ac	5, 7
	Amide (2)	WBE	5, 7

Our study successfully utilized $^{1}H–^{13}C$ NMR spectroscopy to identify potential interaction sites between buffer components and the Fab fragment of the antibody. Spectra of the Fab fragment at pH 5 in different formulations were overlaid, highlighting noteworthy peaks in the aliphatic and aromatic regions (1st and 2nd quadrants) that exhibit distinct chemical shifts compared to the formulation without buffering excipients (Fig. 3). Consistent with our CPMG relaxation measurements, histidine-containing formulations generally induced larger peak shifts than acetate-based formulations. Remaining overlaid spectra are provided in supplementary information (SI) (**Fig. S3**).

While full assignment of the NMR spectrum would provide a comprehensive picture of interactions, it is beyond the scope of this study. However, to strengthen the evidence for spectral differences, a rigorous chemometric analysis was performed.

3.3.3. *Chemometric analysis of methyl fingerprints*

Quantitation of buffer-induced chemical shift perturbations in the $^{1}H–^{13}C$ methyl fingerprint spectra was performed using principal component analysis (PCA), sequential nearest neighbors graph invariants (SNN-GI) and combined chemical shift difference (CCSD).

3.3.3.1. PCA. Principal component analysis scores of the $^{1}H–^{13}C$ methyl fingerprint spectra of the Fab samples at different pH values and in different formulations are visualized (Fig. 4 — **left**). The first 2 principal components were able to account for 61.5 % and 15.3 % of variation in the data, respectively or cumulatively 76,8 % of variation in the X input matrix (**Fig. S4 – left**). Additional 2 principal components, PC3 and PC4 were able to explain 6.4 % and 4.9 % of variation in the data, respectively. The main contributions to the PC1 projection are related to the changes in the pH value. The samples in the pH 5.5 to 7.0 formulations form a relatively compact cluster. The pH 5 (blue samples) are shifted upwards in the PC2 direction. The samples in the pH 9 formulations are forming a cluster, which is the most distant from the other samples suggesting conformational changes in the protein with is the

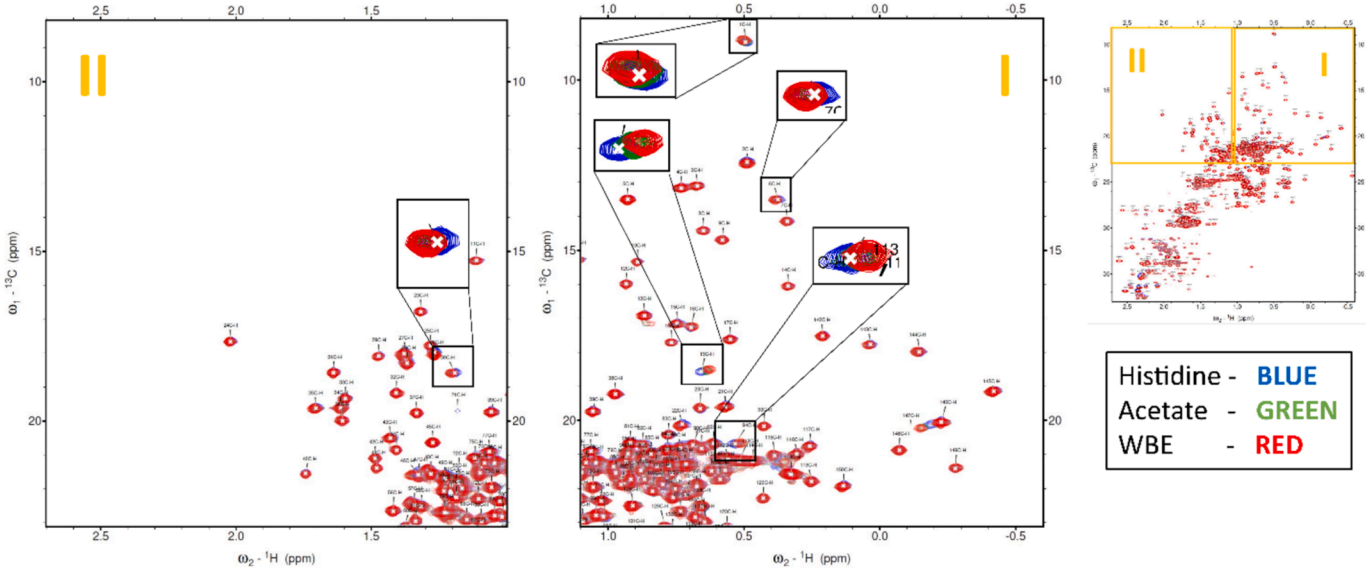

Fig. 3. Overlaid $^{1}H-^{13}C$ NMR spectra of Fab fragment at pH 5, comparing histidine chloride buffer, sodium acetate buffer, and formulation without buffering excipients. Black boxes highlight zoomed-in regions showcasing cross-peaks with notable chemical shift perturbations.

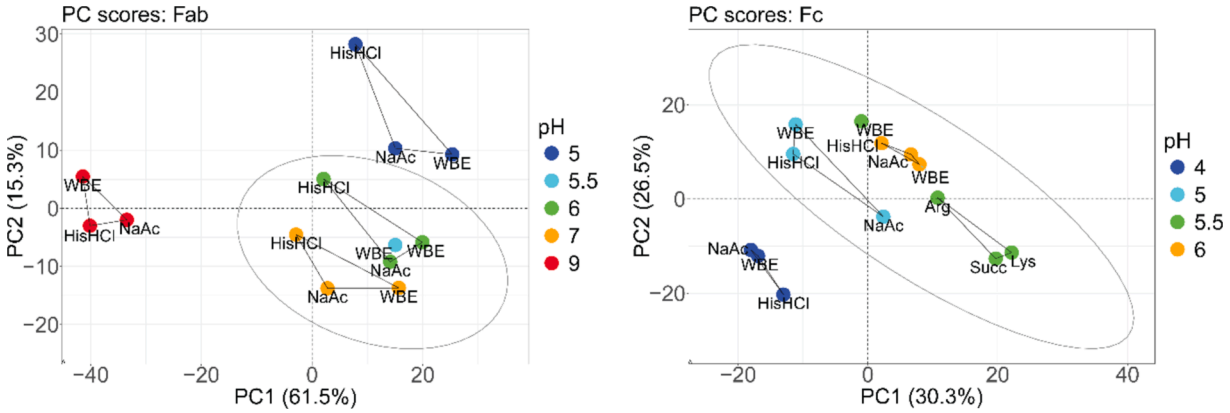

Fig. 4. PCA plot showing the similarity between the Fab (left) and Fc (right) mAb fragments at different pH values (point colors) and in different buffer formulations (histidine chloride buffer (HisHCl), sodium acetate buffer (NaAc) and without buffering excipients (WBE)). The formulation used for each point is specified in the accompanying labels.

most pronounced with increased pH to 9. Overall, the PCA scores are shifted from right to left with increasing pH in the PC1 dimension. Within each pH group a systematic change in the PC scores can be observed (depicted by triangles), which is induced by different formulations. It is interesting to note that the relative orientation of the vertices in the ΔHis/HCl-BL-Na/Ac triangles is the same for the pH values of 5, 6, 7. The only difference is the orientation in the pH 9 sample, which might suggest slightly different behavior in formulation at high pH.

PCA analysis of methyl fingerprint spectra of the Fc samples at different pH values and in different formulations was performed (Fig. 4 – **right**). The first 2 principal components were able to account for 30.3 % and 26.5 % of variation in the data, respectively or cumulatively 56.8 % of variation in the X input matrix (Fig. S4 – **right**). Additional 2 principal components, PC3 and PC4 were able to explain 15.8 % and 7.7 % of variation in the data, respectively. The main contributions to the PC1 projection are related to the changes in the pH value. The samples in the pH of value of 5.0, 5.5 and 6.0 formulations form a cluster, whereas the pH 4 (blue samples) are forming another cluster, which is shifted to the left with respect to PC1 direction. The changes in the higher order structure related to formulations contributes to PC2. Large shifts of the PCA scores in the PC2 direction can be observed for formulation without buffering excipients versus Arg, Lys and succinate formulations.

The PCA score plots results can be interpreted as HOS conformational stability map reflecting the changes in the higher order structure of the protein. The pH 5.5, 6 and 7 Fab samples form a cluster, which is separated from the other pH values indicating relatively small HOS conformational changes at these pH values. The more extreme pH Fab samples (5 and 9) shift away from the pH 5.5, 6 and 7 sample cluster in the PC2 and PC1 direction, respectively. Such map could also be used to measure the systematic shift of the samples due to post-translational modifications if stability timepoints were available.

3.3.3.2. Combined chemical shift deviation (CCSD). The second method, which was used to quantify the difference between spectra, was combined chemical shift deviations, which were calculated according the CCSD equation in the methods section [33,55]. This method has an advantage of quantifying the weighted chemical shift difference at individual peak positions compared to reference. The first set of comparison included buffer comparison where the formulation without buffering excipients was used as a reference formulation, which was compared to histidine chloride and sodium acetate buffer at the same pH

value. The second set of comparison was pH comparison where the reference pH value of 6 was compared to the same buffers at other pH values. The relative CCSD values of the Fab fragment in histidine chloride buffer and sodium acetate buffer versus formulation without buffering excipients at pH 5 for 297 assigned peaks was visualized (Fig. 5 – **A,B**). Regions of sequential peaks can be identified where CCSD values are systematically increased- this may indicate the patches on the protein, which are sensitive to changes in buffer composition. Peak assignment, i.e. residue annotation was not available but rather technical annotation to assure comparison of the same cross peaks, which are lacking the link to a specific residue in the protein.

Histograms of CCSD values in pH5 formulation are shown (Fig. 5 – **C, D**), which confirm the observation (Fig. 4 (PCA score plot)) that the shift in histidine chloride buffer is higher compared to formulation without buffering excipients than in sodium acetate buffer, which is reflected in higher bin counts above the threshold limit of 0.010 ppm. Remaining CCSD histogram comparisons between buffers for the Fab and Fc fragments at different pH values are in shown in SI (**Fig. S5-S7,** respectively). The histograms summarize the distribution of CCSD values rather than calculation the CCSD for each individual crosspeak as was the case for the barplots shown earlier. The threshold of 0.01 ppm would approximately represent 98.5th percentile of the CCSD values in the CDF plot ($i.e. P(X \leq 0.01 ppm) = 0.985$) for the CCDS in the histidine chloride and sodium acetate buffer compared to in formulation without buffering excipients at pH 6.0 and 7.0. Exceeding this threshold indicates conformational changes in the protein.

To show the influence of both pH and buffers on the protein conformation the CCSD comparisons at fixed pH values and fixed buffer were systematically summarized (Fig. 6). The pH significantly influences protein conformation, as observed at various pH levels (5, 6, 7, and 9 for Fab, and 4, 5, 5.5, and 6 for the Fc fragment, respectively) (Fig. 6 – **top**). The pH value of 6 was used as a reference. Both the Fab and the Fc fragments are stable at pH 6.0 (reference spectra) with no shifts in the methyl fingerprint spectra exceeding the threshold value of 0.01 ppm regardless of formulation (without buffering excipients, histidine chloride and sodium acetate buffer). The number of CCSD exceeding the threshold increases above 10 % at pH value of 5 and above 30 % at pH shift of 9 in all three formulations (without buffering

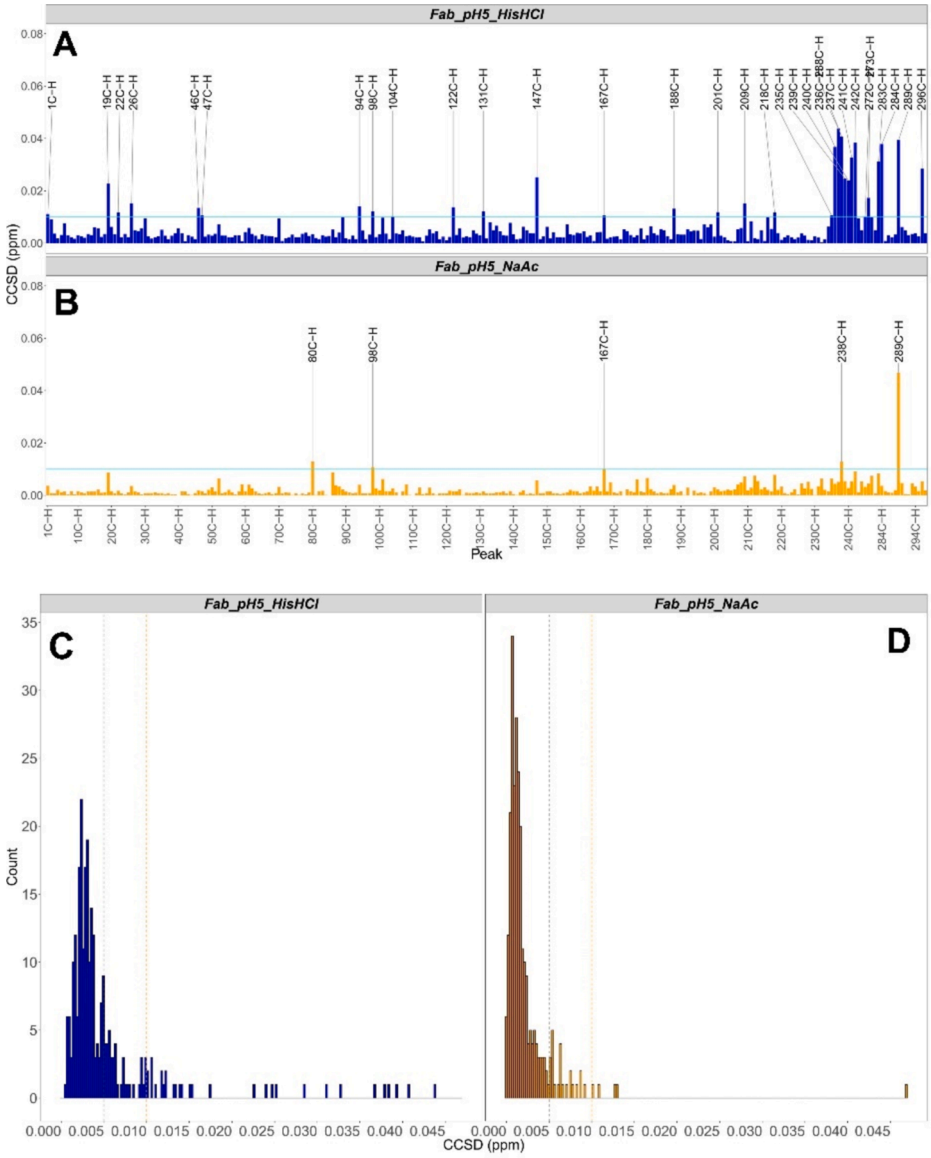

Fig. 5. A, B: CCSD of the individual ^{1}H–^{13}C cross peaks of the Fab samples in histidine chloride (HisHCl) and sodium acetate (NaAc) buffer compared to formulation without buffering excipients (WBE; reference) at pH 5. C, D: CCSD histograms of the Fab samples in HisHCl and NaAc compared to reference formulation without buffering excipients.

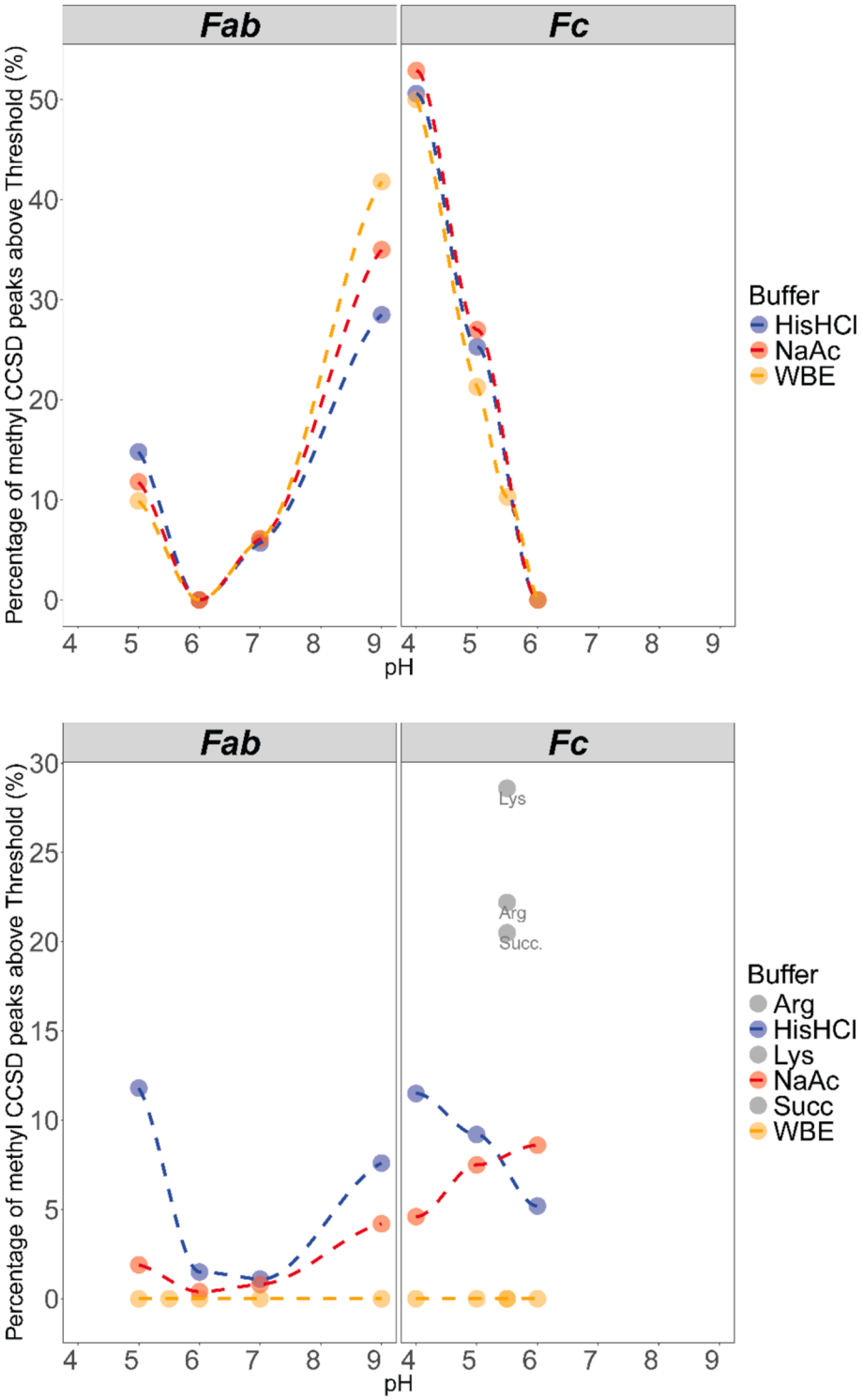

Fig. 6. Top: Percentage of methyl CCSD peaks above the threshold value 0.01 ppm at different pH values normalized to pH value of 6 as a reference for each buffer for the Fab (left) and Fc fragment (right). Bottom: Percentage of methyl CCSD peaks above the threshold value 0.01 ppm at different pH values normalized to formulation without buffering excipients (WBE) as a reference for each pH value. The formulation components are abbreviated as follows: histidine chloride buffer (HisHCl), sodium acetate buffer (NaAc), arginine (Arg), lysine (Lys), succinic acid (Succ), and formulations without buffering excipients (WBE).

excipients, sodium acetate and histidine chloride buffer). It is interesting to note that there is the reverse switch in the buffer effect from low to high pH: at low pH the number of histidine chloride CCSD exceeding the threshold is the highest while at pH value of 9 the number of histidine chloride buffer CCSD exceeding the threshold is lower compared to sodium acetate buffer and formulation without buffering excipients. This is not surprising considering the theoretical pI values of Fab and Fc (8.89 and 8.02 respectively calculated using Expasy protparam tool) [56].

The buffer effect is also shown (Fig. 6 **– bottom)**. The CCSD values in the histidine chloride and sodium acetate buffer compared to formulation without buffering excipients of the Fab fragment showed relatively small number of cross peaks at pH value of 6, which exceeded the threshold of 0.01 ppm (4/263 (1.5 %) and 1/263 (0.4 %) in histidine chloride and sodium acetate buffer respectively. This percentage is

increased at pH value of 5 to 31/263 (11.8 %) and 5/263 (1.9 %) in histidine chloride and sodium acetate buffer respectively. Similar trend is observed with pH values of 7 and 9. The Fab fragment seems to have high conformational stability at pH 6 and 7 irrespective of the buffer. The Fc fragment seems to be more stable in the sodium acetate buffer at low pH values while the stability increases in histidine chloride buffer at higher pH. The experiments were performed in the pH range 4 to 6 due to problem with solubility of the Fc fragment at higher pH values.

Comparison of the CCSD of the Fc sample with arginine, lysine and succinate versus formulation without buffering excipients showed increased number of peaks exceeding the CCSD threshold of 0.01 ppm (53/185 for Lys, 41/185 for Arg and 38/185 for succinate buffers, respectively) (Fig. 6 – bottom right and **Fig S6**). The effect of these buffers is probably due to increased interactions with Fc fragment since stabilization effects were observed (Table 1).

3.3.3.3. SNN-GI. The third method, which was used to characterize the methyl fingerprints in different formulations, was sequential nearest neighbors graph invariants (SNN-GI) [52,53]. This method uses a set of map invariants (numerical descriptors), which do not depend neither on numbering of protein signals nor on the orientation of the protein map. Each spot is numbered according to relative abundance (peak intensity) and connected to its nearest neighbors of a lower order. The SNN-GI plot of Fab methyl spectra is shown in SI (**Fig. S8 – A-F**). Systematic differences were observed between the samples at different pH values in different buffers. Similar to PCA analysis the pH contributes more to separation than buffers splitting the samples into 2 distinct groups (pH 5,6,7 versus pH 9) with respect to magnitude of individual rows sums (**Fig. S9-F**). The SNN-GI plot of Fc methyl spectra is shown in SI (**Fig. S9**). Systematic differences are observed between the samples at different pH values. Overall SNN-GI seems is to be less sensitive compared to PCA and CCSD methods.

3.3.4. Amide fingerprinting

Similar to methyl fingerprinting, amide fingerprinting offers valuable insights into the chemical environment of amide groups and the HOS of proteins. Despite the lower natural abundance of ^{15}N compared to ^{13}C (0.4 % versus 1.109 %), leading to longer acquisition times (24 h in this study), it still generates spectra with satisfactory resolution. Due to these time constraints, only the Fab fragment in acetate buffer at pH 5 and 7 were analyzed. Spectral overlays and subsequent chemometric analysis were performed.

Overlaid $^{1}H–^{15}N$ spectra of the Fab fragment at pH 7 are presented, highlighting peaks in the 4th quadrant exhibiting apparent chemical shifts in the presence of acetate buffer (Fig. 7). Additional overlaid spectra are included in SI (**Fig. S10**). These initial observations are further evaluated and validated through chemometric analysis in a later section.

The analysis of CCSD from amide fingerprint experiments is shown in SI (**Fig S11**). In order to explore the influence of buffer on HOS the Fab fragment in NaAc buffer was compared to formulation without buffering excipients at pH 5 and 7. The comparison in both buffers showed 11.8 and 13.2 % of CCSD exceeding the threshold value of 0.01 ppm indicating that the buffer has an influence on the HOS. The threshold value of 0.01 ppm is stricter in amide than methyl fingerprint spectra corresponding to the coverage of approximately 88 %. The threshold for the 98.5 % coverage, which was used in methyl fingerprint spectra, would be ~0.025 ppm in the amide fingerprint spectra indicating the amide fingerprints are approximately 2–3 times more sensitive to CCSD changes compared to methyl fingerprints.

3.3.5. MD simulations

The results obtained from the molecular dynamics (MD) simulations indicate that histidine and acetate molecules are found to be in closer proximity to certain regions of the protein compared to others. Specifically, when they are near methyl groups present in the side chains of six amino acids (A, V, L, I, M, T; Fig. 8, colored red), any changes in the chemical environment of these methyl groups lead to a shift in the peaks observed in the 2D NMR spectra. (section 3.3.2). Results of the simulations of both Fab and Fc fragments with histidine and acetic acid are presented here (Fig. 8).

The figure provided shows the simulation box containing one Fab or Fc fragment, with the protonation states of the titratable protein groups determined using PROPKA3.5 with pH set to corresponding pH value. Additionally, the simulation box includes the specific number of charged buffer species as determined by Henderson-Hasselbalch Equation. For example, with fragment Fab at pH 5 in histidine buffer, 17 histidine molecules are present in total – 15 positive (+1 charge) and two neutral (0 state). This methodology was applied to accurately simulate the state of these molecules in a real solution of histidine and acetic acid formulations for all other tested pH values. The surface of the mAb fragments is colored in purple, with the intensity set according to the level of interaction with all histidine molecules in the simulation box (procedure described in section 2.8.2). In regions where the higher *in silico* derived level of interaction (purple) coincides with the methyl group spots in the figure (red), perturbations of the methyl fingerprint can be expected. It

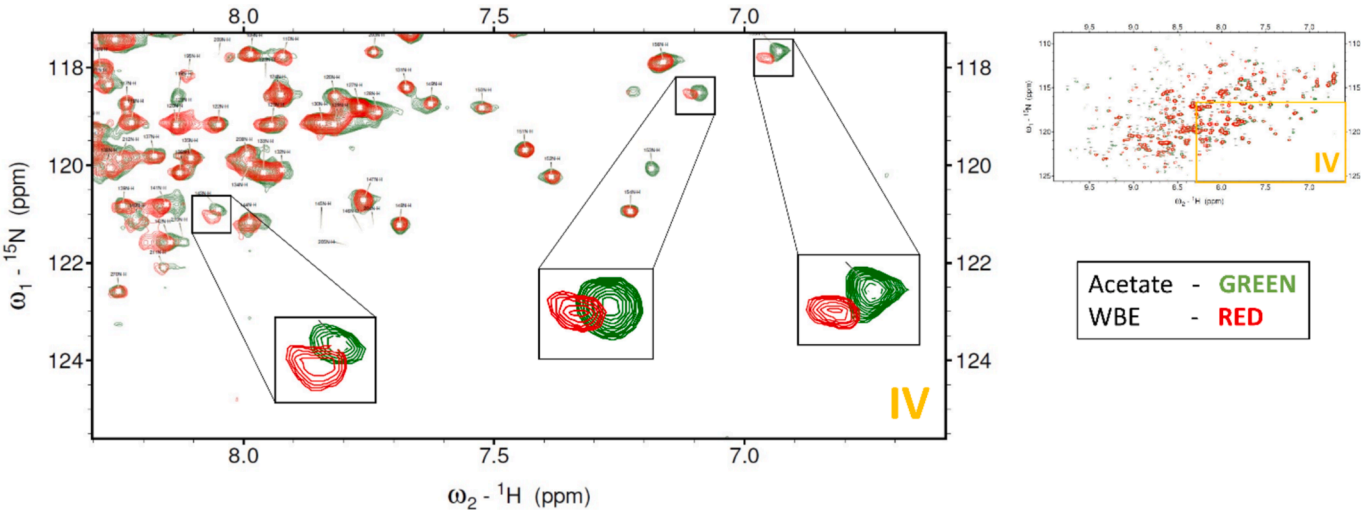

Fig. 7. Overlaid $^{1}H–^{15}N$ NMR spectra of the Fab fragment (focusing on the 4th quadrant) at pH 7, comparing sodium acetate buffer and formulation without buffering excipients (WBE). Black boxes highlight zoomed-in regions showcasing amide peaks with notable chemical shift perturbations.

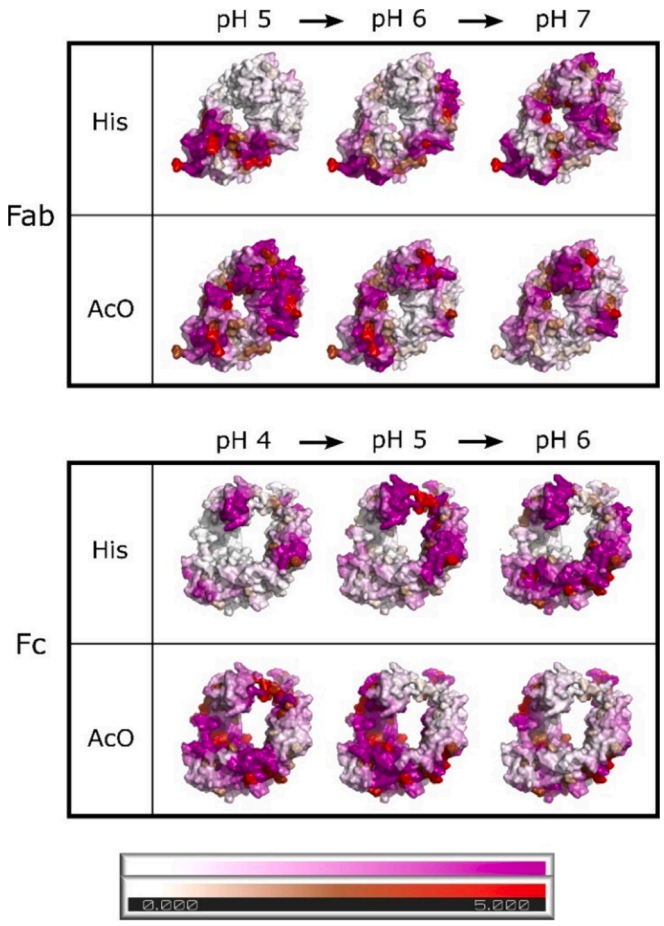

Fig. 8. Fab and Fc fragments' interactions with histidine (His) and acetate (AcO) molecules at different pH. White-purple color scale represents level of interaction (more intense color means higher level of interaction), while methyl sites are further differentiated using a white-brown–red color scale. (For interpretation of the references to color in this figure legend, the reader is referred to the web version of this article.)

is important to note that the simulation results cannot be directly applied to the NMR spectra, as the assignation of the latter was not performed.

4. Conclusions

Protein-buffer interactions play a key role in biopharmaceutical formulation stability, yet their weak and transient nature makes them difficult to characterize. This study demonstrates the effectiveness of combining complementary analytical methods to investigate these interactions. Our results show that even a simple 1D NMR CPMG experiment can detect interactions and support observations related to Fc instability and stabilizer efficiency. Furthermore, methyl and amide fingerprinting at the natural abundance of ^{13}C and ^{15}N proved sensitive in revealing these interactions. Though slightly less sensitive to chemical shift changes, methyl fingerprinting offers the advantage of shorter experiment duration. While we did not perform full 2D NMR spectra assignment, we established the method's potential for unambiguously identifying contacts. Chemometric methods (PCA and CCSD) effectively detected spectral differences, thus highlighting their utility in evaluating protein-excipient interactions. Despite 2D NMR capability of detecting weak interactions related to HOS perturbations, these NMR techniques have limitations, such as long experiment times, lower resolution, consequently requiring mAb cleavage into Fab and Fc fragments, making them less practical for routine use. Interaction strength was too low for detection with the SNN-GI method. Overall, this work advances the field towards a rational-based formulation design strategy, moving away from traditional trial-and-error approaches.

CRediT authorship contribution statement

Blaž Lebar: Writing – review & editing, Writing – original draft, Visualization, Validation, Supervision, Software, Resources, Project administration, Methodology, Investigation, Formal analysis, Data curation, Conceptualization. **Maria Orehova:** Writing – original draft, Validation, Methodology, Investigation. **Boštjan Japelj:** Writing – original draft, Visualization, Software, Resources, Methodology, Investigation, Funding acquisition, Formal analysis, Data curation, Conceptualization. **Ernest Šprager:** Writing – original draft, Visualization, Methodology, Investigation. **Rok Podlipec:** Writing – original draft, Visualization, Formal analysis. **Tilen Knaflič:** Writing – original draft, Investigation. **Iztok Urbančič:** Writing – review & editing, Methodology, Formal analysis. **Benjamin Knez:** Writing – original draft, Visualization, Software, Methodology, Investigation, Formal analysis. **Mitja Zidar:** Supervision, Software, Methodology. **Jure Cerar:** Supervision, Software, Resources, Methodology. **Janez Mravljak:** Writing – review & editing, Visualization, Validation. **Aleš Žula:** Funding acquisition. **Denis Arčon:** Project administration, Funding acquisition. **Janez Plavec:** Writing – review & editing, Visualization, Validation. **Stane Pajk:** Writing – review & editing, Visualization, Validation, Supervision, Resources, Project administration, Methodology, Investigation, Funding acquisition, Conceptualization.

Declaration of competing interest

The authors declare that they have no known competing financial interests or personal relationships that could have appeared to influence the work reported in this paper.

Acknowledgments

This work was supported by Novartis Pharmaceutical Manufacturing LLC and the Slovenian Research and Innovation Agency (core research funding P1-0208).

Appendix A. Supplementary material

Supplementary data to this article can be found online at https://doi.org/10.1016/j.ejpb.2024.114582.

Data availability

Data will be made available on request.

References

[1] G. Walsh, Biopharmaceutical benchmarks, Nat. Biotechnol. 36 (2018) (2018) 1136–1145, https://doi.org/10.1038/nbt.4305.
[2] S. Uchiyama, Liquid formulation for antibody drugs, Biochim. Biophys. Acta 1844 (2014) 2041–2052, https://doi.org/10.1016/j.bbapap.2014.07.016.
[3] S.J. Shire, Monoclonal Antibodies: Meeting the Challenges in Manufacturing, Formulation, Delivery and Stability of Final Drug Product, Woodhead Publishing, 2015.
[4] F. Jameel, S. Hershenson, in: Formulation and Process Development Strategies for Manufacturing Biopharmaceuticals, John Wiley & Sons, 2010, https://doi.org/10.1002/9780470595886.
[5] P. Garidel, A. Blume, M. Wagner, Prediction of colloidal stability of high concentration protein formulations, Pharm. Dev. Technol. 20 (2015) 367–374, https://doi.org/10.3109/10837450.2013.871032.
[6] I. Ghosh, H. Gutka, M.E. Krause, R. Clemens, R.S. Kashi, A systematic review of commercial high concentration antibody drug products approved in the US: formulation composition, dosage form design and primary packaging considerations, Mabs 15 (2023) 2205540, https://doi.org/10.1080/19420862.2023.2205540.

[7] S.O. Ugwu, S.P. Apte, The Effect of Buffers on Protein Conformational Stability, Pharm. Technol. 81 (2004) 339–352, https://doi.org/10.1016/j.saa.2011.06.021.
[8] T.J. Zbacnik, R.E. Holcomb, D.S. Katayama, B.M. Murphy, R.W. Payne, R. C. Coccaro, G.J. Evans, J.E. Matsuura, C.S. Henry, M.C. Manning, Role of buffers in protein formulations, J. Pharm. Sci. 106 (2017) 713–733, https://doi.org/10.1016/j.xphs.2016.11.014.
[9] J.Y. Zheng, L.J. Janis, Influence of pH, buffer species, and storage temperature on physicochemical stability of a humanized monoclonal antibody LA298, Int. J. Pharm. 308 (2006) 46–51, https://doi.org/10.1016/j.ijpharm.2005.10.024.
[10] O. Esue, S. Kanai, J. Liu, T.W. Patapoff, S.J. Shire, Carboxylate-dependent gelation of a monoclonal antibody, Pharm. Res. 26 (2009) 2478–2485, https://doi.org/10.1007/s11095-009-9963-6.
[11] T.J. Kamerzell, R. Esfandiary, S.B. Joshi, C.R. Middaugh, D.B. Volkin, Protein-excipient interactions: Mechanisms and biophysical characterization applied to protein formulation development, Adv. Drug Deliv. Rev. 63 (2011) 1118–1159, https://doi.org/10.1016/j.addr.2011.07.006.
[12] M. Zidar, Analysis and Prediction of Aggregation and Degradation in Protein-Based Biopharmaceuticals, Doctoral Dissertation, University of Ljubljana, 2020.
[13] K. Shiraki, M. Kudou, S. Fujiwara, T. Imanaka, M. Takagi, Biophysical effect of amino acids on the prevention of protein aggregation, J. Biochem. 132 (2002) 591–595, https://doi.org/10.1093/oxfordjournals.jbchem.a003261.
[14] T. Arakawa, K. Tsumoto, The effects of arginine on refolding of aggregated proteins: not facilitate refolding, but suppress aggregation, Biochem. Biophys. Res. Commun. 304 (2003) 148–152, https://doi.org/10.1016/s0006-291x(03)00578-3.
[15] C. Lange, R. Rudolph, Suppression of protein aggregation by L-arginine, Curr. Pharm. Biotechnol. 10 (2009) 408–414, https://doi.org/10.2174/138920109788488851.
[16] T. Arakawa, D. Ejima, K. Tsumoto, N. Obeyama, Y. Tanaka, Y. Kita, S.N. Timasheff, Suppression of protein interactions by arginine: A proposed mechanism of the arginine effects, Biophys. Chem. 127 (2007) 1–8, https://doi.org/10.1016/j.bpc.2006.12.007.
[17] D. Shukla, B.L. Trout, Preferential interaction coefficients of proteins in aqueous arginine solutions and their molecular origins, J. Phys. Chem. B 115 (2011) 1243–1253, https://doi.org/10.1021/jp108586b.
[18] B.M. Baynes, D.I.C. Wang, B.L. Trout, Role of arginine in the stabilization of proteins against aggregation, Biochemistry 44 (2005) 4919–4925, https://doi.org/10.1021/bi047528r.
[19] L. Wen, X. Zheng, X. Wang, H. Lan, Z. Yin, Bilateral effects of excipients on protein stability: preferential interaction type of excipient and surface aromatic hydrophobicity of protein, Pharm. Res. 34 (2017) 1378–1390, https://doi.org/10.1007/s11095-017-2152-0.
[20] D. Shukla, B.L. Trout, Interaction of arginine with proteins and the mechanism by which it inhibits aggregation, J. Phys. Chem. B 114 (2010) 13426–13438, https://doi.org/10.1021/jp108399g.
[21] C. Harinarayan, K. Skidmore, Y. Kao, A.L. Zydney, R. Van Reis, Small molecule clearance in ultrafiltration/diafiltration in relation to protein interactions: Study of citrate binding to a fab, Biotechnol. Bioeng. 102 (2009) 1718–1722, https://doi.org/10.1002/bit.22196.
[22] R. Fayos, M. Pons, O. Millet, On the origin of the thermostabilization of proteins induced by sodium phosphate, J. Am. Chem. Soc. 127 (2005) 9690–9691, https://doi.org/10.1021/ja051352e.
[23] D. McPhail, C. Holt, Effect of anions on the denaturation and aggregation of β-Lactoglobulin as measured by differential scanning microcalorimetry, Int. J. Food Sci. Technol. 34 (1999) 477–481, https://doi.org/10.1046/j.1365-2621.1999.00316.x.
[24] S. Deechongkit, J. Wen, L.O. Narhi, Y. Jiang, S.S. Park, J. Kim, B.A. Kerwin, Physical and biophysical effects of polysorbate 20 and 80 on darbepoetin alfa, J. Pharm. Sci. 98 (2009) 3200–3217, https://doi.org/10.1002/jps.21740.
[25] N.B. Bam, Tween protects recombinant human growth hormone against agitation-induced damage via hydrophobie interactions, J. Pharm. Sci. 87 (1998) 1554–1559, https://doi.org/10.1021/js980175v.
[26] F. Tian, C.R. Middaugh, T. Offerdahl, E. Munson, S. Sane, J.H. Rytting, Spectroscopic evaluation of the stabilization of humanized monoclonal antibodies in amino acid formulations, Int. J. Pharm. 335 (2007) 20–31, https://doi.org/10.1016/j.ijpharm.2006.10.037.
[27] W. Maeder, P. Lieby, A. Sebald, M. Spycher, R. Pedrussio, R. Bolli, Local tolerance and stability up to 24 months of a new 20% proline-stabilized polyclonal immunoglobulin for subcutaneous administration, Biologicals 39 (2011) 43–49, https://doi.org/10.1016/j.biologicals.2010.11.004.
[28] P. Kheddo, M.J. Cliff, S. Uddin, C.F. van der Walle, A.P. Golovanov, Characterizing monoclonal antibody formulations in arginine glutamate solutions using 1H NMR spectroscopy, Mabs 8 (2016) 1245–1258, https://doi.org/10.1080/19420862.2016.1214786.
[29] S.G. Patching, Surface plasmon resonance spectroscopy for characterisation of membrane protein-ligand interactions and its potential for drug discovery, Biochim. Biophys. Acta 1838 (2014) 43–55, https://doi.org/10.1016/j.bbamem.2013.04.028.
[30] X. Du, Y. Li, Y.L. Xia, S.M. Ai, J. Liang, P. Sang, X.L. Ji, S.Q. Liu, Insights into protein–ligand interactions: Mechanisms, models, and methods, Int. J. Mol. Sci. 17 (2016), https://doi.org/10.3390/ijms17020144.
[31] M. Zalar, H.L. Svilenov, A.P. Golovanov, Binding of excipients is a poor predictor for aggregation kinetics of biopharmaceutical proteins, Eur. J. Pharm. Biopharm. 151 (2020) 127–136, https://doi.org/10.1016/j.ejpb.2020.04.002.
[32] L.W. Arbogast, R.G. Brinson, J.P. Marino, Mapping monoclonal antibody structure by 2D 13C NMR at natural abundance, Anal. Chem. 87 (2015) 3556–3561, https://doi.org/10.1021/ac504804m.
[33] R.G. Brinson, J.P. Marino, F. Delaglio, L.W. Arbogast, R.M. Evans, A. Kearsley, G. Gingras, H. Ghasriani, Y. Aubin, G.K. Pierens, X. Jia, M. Mobli, H.G. Grant, D. W. Keizer, K. Schweimer, J. Ståhle, G. Widmalm, E.R. Zartler, C.W. Lawrence, P. N. Reardon, J.R. Cort, P. Xu, F. Ni, S. Yanaka, K. Kato, S.R. Parnham, D. Tsao, A. Blomgren, T. Rundlöf, N. Trieloff, P. Schmieder, A. Ross, K. Skidmore, K. Chen, D. Keire, D.I. Freedberg, T. Suter-Stahel, G. Wider, G. Ilc, J. Plavec, S.A. Bradley, D. M. Baldisseri, M.L. Sforça, A.C. de M. Zeri, J.Y. Wei, C.M. Szabo, C.A. Amezcua, J. B. Jordan, M. Wikström, Enabling adoption of 2D-NMR for the higher order structure assessment of monoclonal antibody therapeutics, Mabs 11 (2019) 94–105, https://doi.org/10.1080/19420862.2018.1544454.
[34] S.M. Singh, S. Bandi, D.N.M. Jones, K.M.G. Mallela, Effect of polysorbate 20 and polysorbate 80 on the higher-order structure of a monoclonal antibody and its fab and fc fragments probed using 2D nuclear magnetic resonance spectroscopy, J. Pharm. Sci. 106 (2017) 3486–3498, https://doi.org/10.1016/j.xphs.2017.08.011.
[35] Y. Aubin, D.J. Hodgson, W.B. Thach, G. Gingras, S. Sauvé, Monitoring effects of excipients, formulation parameters and mutations on the high order structure of filgrastim by NMR, Pharm. Res. 32 (2015) 3365–3375, https://doi.org/10.1007/s11095-015-1713-3.
[36] J. Panchal, B.T. Falk, V. Antochshuk, M.A. McCoy, Investigating protein-excipient interactions of a multivalent V(HH) therapeutic protein using NMR spectroscopy, Mabs 14 (2022) 2124902, https://doi.org/10.1080/19420862.2022.2124902.
[37] D. Shukla, C. Shinde, B.L. Trout, Molecular computations of preferential interaction coefficients of proteins, J. Phys. Chem. B 113 (2009) 12546–12554, https://doi.org/10.1021/jp810949t.
[38] T. Cloutier, C. Sudrik, N. Mody, H.A. Sathish, B.L. Trout, Molecular computations of preferential interaction coefficients of IgG1 monoclonal antibodies with sorbitol, sucrose, and trehalose and the impact of these excipients on aggregation and viscosity, Mol. Pharm. 16 (2019) 3657–3664, https://doi.org/10.1021/acs.molpharmaceut.9b00545.
[39] T.K. Cloutier, C. Sudrik, N. Mody, S.A. Hasige, B.L. Trout, Molecular computations of preferential interactions of proline, arginine.HCl, and NaCl with IgG1 antibodies and their impact on aggregation and viscosity, Mabs 12 (2020) 1–12, https://doi.org/10.1080/19420862.2020.1816312.
[40] N. Chennamsetty, V. Voynov, V. Kayser, B. Helk, B.L. Trout, Design of therapeutic proteins with enhanced stability, Proc. Natl. Acad. Sci. U. S. A. 106 (2009) 11937–11942, https://doi.org/10.1073/pnas.0904191106.
[41] N.J. Agrawal, B. Helk, S. Kumar, N. Mody, H.A. Sathish, H.S. Samra, P.M. Buck, L. Li, B.L. Trout, Computational tool for the early screening of monoclonal antibodies for their viscosities, Mabs 8 (2016) 43–48, https://doi.org/10.1080/19420862.2015.1099773.
[42] S. Saurabh, C. Kalonia, Z. Li, P. Hollowell, T. Waigh, P. Li, J. Webster, J.M. Seddon, J.R. Lu, F. Bresme, Understanding the stabilizing effect of histidine on mab aggregation: a molecular dynamics study, Mol. Pharm. 19 (2022) 3288–3303, https://doi.org/10.1021/acs.molpharmaceut.2c00453.
[43] E.O. Saphire, P.W. Parren, R. Pantophlet, M.B. Zwick, G.M. Morris, P.M. Rudd, R. A. Dwek, R.L. Stanfield, D.R. Burton, I.A. Wilson, Crystal structure of a neutralizing human IGG against HIV-1: a template for vaccine design, Science 293 (2001) 1155–1159, https://doi.org/10.1126/science.1061692.
[44] K. Zhu, T. Day, D. Warshaviak, C. Murrett, R. Friesner, D. Pearlman, Antibody structure determination using a combination of homology modeling, energy-based refinement, and loop prediction, Proteins 82 (2014) 1646–1655, https://doi.org/10.1002/prot.24551.
[45] M. Abraham, T. Murtola, R. Schulz, S. Páll, J. Smith, B. Hess, E. Lindahl, GROMACS: High performance molecular simulations through multi-level parallelism from laptops to supercomputers, SoftwareX 1 (2015), https://doi.org/10.1016/j.softx.2015.06.001.
[46] M.J. Robertson, J. Tirado-Rives, W.L. Jorgensen, Improved Peptide and Protein Torsional Energetics with the OPLS-AA Force Field, J. Chem. Theory Comput. 11 (2015) 3499–3509, https://doi.org/10.1021/acs.jctc.5b00356.
[47] W. Jorgensen, J. Chandrasekhar, J. Madura, R. Impey, M. Klein, Comparison of simple potential functions for simulating liquid water, J. Chem. Phys. 79 (1983) 926–935, https://doi.org/10.1063/1.445869.
[48] M.H.M. Olsson, C.R. Søndergaard, M. Rostkowski, J.H. Jensen, PROPKA3: Consistent Treatment of Internal and Surface Residues in Empirical pKa Predictions, J. Chem. Theory Comput. 7 (2011) 525–537, https://doi.org/10.1021/ct100578z.
[49] N. Michaud-Agrawal, E.J. Denning, T.B. Woolf, O. Beckstein, MDAnalysis: a toolkit for the analysis of molecular dynamics simulations, J. Comput. Chem. 32 (2011) 2319–2327, https://doi.org/10.1002/jcc.21787.
[50] A. Kassambra, F. Mundt, factoextra : Extract and Visualize the Results of Multivariate Data Analyses, (2020). https://rpkgs.datanovia.com/factoextra/.
[51] A. R Foundation for Statistical Computing, Vienna, R Core Team. R: A language and environment for statistical computing, (2022). https://www.r-project.org/.
[52] M. Randić, M. Novic, M. Vracko, Novel characterization of proteomics maps by sequential neighborhoods of protein spots, J. Chem. Inf. Model. 45 (2005) 1205–1213, https://doi.org/10.1021/ci0497612.
[53] K. Chen, J. Park, F. Li, S.M. Patil, D.A. Keire, Chemometric methods to quantify 1D and 2D NMR spectral differences among similar protein therapeutics, AAPS PharmSciTech 19 (2018) 1011–1019, https://doi.org/10.1208/s12249-017-0911-1.

[54] B. Hobbs, J. Drant, M.P. Williamson, The measurement of binding affinities by NMR chemical shift perturbation, J. Biomol. NMR 76 (2022) 153–163, https://doi.org/10.1007/s10858-022-00402-3.
[55] H. Ghasriani, D.J. Hodgson, R.G. Brinson, I. McEwen, L.F. Buhse, S. Kozlowski, J. P. Marino, Y. Aubin, D.A. Keire, Precision and robustness of 2D-NMR for structure assessment of filgrastim biosimilars, Nat. Biotechnol. 34 (2016) 139–141, https://doi.org/10.1038/nbt.3474.
[56] E. Gasteiger, C. Hoogland, A. Gattiker, S. Duvaud, M.R. Wilkins, R.D. Appel, A. Bairoch, Protein Identification and Analysis Tools on the ExPASy Server BT - The Proteomics Protocols Handbook, in: J.M. Walker (Ed.), Humana Press, Totowa, NJ, 2005: pp. 571–607. Doi: 10.1385/1-59259-890-0:571.